High Resolution MR Images from 3T Active-Shield Whole-Body MRI System

Bo-Young Choe[1], Sei-Kwon Kang[1], Myoung-Ja Chu[1], Hyun-Man Baik[1], Euy-Neyng Kim[2], Bum-Soo Kim[2], Jae-Mun Lee[2], Sung-Taek Chung[3], Chang-Beom Ahn[4], Chang-Hyun Oh[5], Jung-Ho Kim[6], Sun-Il Kim[7], Keun-Nam Lee[8], Tae-Suk Suh[1], Hyoung-Koo Lee[1], Heung-Kyu Lee[1], Kyung-Sub Shinn[1,2]

Purpose : Within a clinically acceptable time frame, we obtained the high resolution MR images of the human brain, knee, foot and wrist from 3T whole-body MRI system which was equipped with the world first 3T active shield magnet.

Materials and Methods : Spin echo (SE) and Fast Spin Echo (FSE) images were obtained from the human brain, knee, foot and wrist of normal subjects using a homemade birdcage and transverse electromagnetic (TEM) resonators operating in quadrature and tuned to 128 MHz. For acquisition of MR images of knee, foot and wrist, we employed a homemade saddle shaped RF coil. Typical common acquisition parameters were as follows: matrix = 512 × 512, field of view (FOV) = 20 cm, slice thickness = 3 mm, number of excitations (NEX) = 1. For T1-weighted MR images, we used TR = 500 ms, TE = 10 or 17.4 ms. For T2-weighted MR images, we used TR = 4000 ms, TE = 108 ms.

Results : Signal to noise ratio (SNR) of 3T system was measured 2.7 times greater than that of prevalent 1.5T system. MR images obtained from 3T system revealed numerous small venous structures throughout the image plane and provided reasonable delineation between gray and white matter.

Conclusion : The present results demonstrate that the MR images from 3T system could provide better diagnostic quality of resolution and sensitivity than those of 1.5T system. The elevated SNR observed in the 3T high field magnetic resonance imaging can be utilized to acquire images with a level of resolution approaching the microscopic structural level under in vivo conditions. These images represent a significant advance in our ability to examine small anatomical features with noninvasive imaging methods.

Index words : Magnetic resonance imaging, High field, High resolution

JKSMRM 5:138-148(2001)

[1]Departments of Biomedical Engineering and [2]Radiology, Kangnam St. Mary's Hospital, College of Medicine, The Catholic University of Korea, [3]Medinus Co. [4]Department of Electrical Engineering, Kwangwoon University, [5]Department of Electronics and Information Engineering, Korea University, [6]Department of Electrical Engineering, KAIST, [7]Department of Hanyang Institute of Technology, Hanyang University, [8]Dongbo System Co.

This study was supported by the Research Fund of Generic Industrial Technology Program (B31-973-3302-01-1-4) in Korean Ministry of Commerce, Industry and Energy.

Received; August 10, 2001, acceepted; October 6, 2001

Address reprint requests to : Bo-Young Choe, Ph.D., Department of Biomedical Engineering, Kangnam St. Mary's Hospital, College of Medicine, The Catholic University of Korea, #505 Banpo-Dong, Seocho-Gu, Seoul 137-040, Korea
Tel. 82-2-590-2427, Fax. 82-2-590-2425, E-mail: bychoe@cmc.cuk.ac.kr

Introduction

The first magnetic resonance imaging experiments were conducted with nuclear magnetic resonance (NMR) line scanning (1) and projection reconstruction (2) methods. While these methods established the feasibility of the magnetic resonance imaging (MRI) approach, they were characterized with relatively low spatial resolution (1, 2). Nonetheless, technological achievable spatial resolution gradient design (3) and spatial encoding methods (4, 5) soon permitted an increase in achievable spatial resolution, thereby greatly improving the radiological utility of MRI methods.

The need for enhanced spatial resolution in magnetic resonance arises from the desire to more precisely visualize small structures both on conventional and angiographic images. Increased spatial resolution also results in reduced susceptibility artifacts echo based MR imaging in part due to the associated increases in receiver bandwidths (6, 7). In addition, enhanced spatial resolution leads to superior image interpolation required in generating MR angiograms (MRA).

Unfortunately, since magnetic resonance is an inherent technique, image resolution cannot be continuously increased without significantly compromising image quality and signal to noise (8-11). As these two characteristics progressively deteriorate, the ability to detect the structure of interest, or the visibility, also degrades. Visibility (V) can be defined as the product of the contrast-to-noise ratio (CNR) and the square root of the number of pixels (p) occupied by the object of interest. It is expressed as follows:$V = CNR\ p$. The importance of determining appropriate spatial resolution based on visibility rather than signal-to-noise criteria alone has been addressed (12).

At 1.5T, increases in spatial resolution have often been associated with the use of specialized local surface (13) or phased array (14) radio frequency (RF) coils in order to maximize the available signal, to noise at this field strength. In addition, signal processing methods may help enhance signal to noise while preserving, as much as possible, edge definition (15-16). Using a combination of these approaches, excellent high resolution images have been obtained from the human skin (17), the extremities and cartilage (18-20), the trabecular bone (21-22), the inner ear (23-27), the eye (28-31), and the facial nerves (32-34). Increased spatial resolution has also proven valuable in MRA studies where higher resolution 3D data sets provide vessel visualization (35-36). Indeed, increased spatial resolution leads not only to the visualization of more vessels but also in the ability to differentiate progressively smaller structures. It is known for instance that vessel visibility is determined by the position of the structure of interest within the voxel grid (37). Vessels contained entirely within one voxel are thus brighter than when positioned between voxels. This is a partial volume effect that can be reduced with increased matrix size. Nonetheless, as resolution continues to increase, signal to noise to degrade to such an extent that visibility becomes compromised and the number of vessels observed no longer continues to increase. Similarly, while high resolution approaches increase functional localization in functional MRI by reducing partial volume effects, this is associated both with a significant increase in scan times and a reduction in signal to noise (38).

Despite limitations in signal to noise even with high field systems operating at 1.5T, excellent high resolution studies of the human brain have been conducted at this field strength. Using phased array detectors and an automated intensity correction algorithm, for instance, Wald et al. (39) have been able to obtain good spoiled gradient recalled volume acquisition images. In these studies, an in-plane pixel size of 0.47-0.66 mm was obtained using a 0.7 mm slice thickness. Alternatively, using a fast spin echo approach were able to obtain 512×512 images with an in-plane resolution of 0.27-0.33 mm with a 1.5-3 mm slice thickness and an acquisition time of only 8.5 minutes. Similarly, Feinberg et al. (40) using the gradient-SE (GRASE) technique and partial k-space sampling, were able to obtain 2D-1024 matrix images of the human head in only 4 minutes, 20 seconds. The resulting images contained a 0.28×0.27 mm in-plan resolution and displayed many small anatomic structures including the cochlea of the inner ear, vascular details, and the cranial nerves.

Given available field strength and total acquisition time, the aforementioned studies illustrate the potential of high resolution MRI. This conclusion can be further amplified by work performed at 4T (41-42) where high

resolution modified driven equilibrium Fourier transform (MDEFT) images were obtained using a 512 $\times$512 matrix. These images had a 400-500 μm in-plane resolution from a 5 mm slice and revealed exquisite anatomical detail and gray/white matter contrast. Moreover, they display remarkable signal to noise in very high field (VHF) MRI, despite the use of standard volumetric head coils (43).

Recently, a series of 1K$\times$1K gradient echo images with a 200 μm in-plane resolution (44-45) have been obtained from the human head at 8 Tesla (46-47) using standard transverse electromagnetic (TEM) volumetric coils (48). These images display good in-plane resolution and enhancement of the venous vasculature. In addition, they highlight the tremendous magnetic susceptibility obtained at ultra high field strengths.

Materials and Methods

High resolution gradient recalled echo images were acquired at 128 MHz using a 3T instrument. It consists of a 3 Tesla/64 cm superconducting magnet manufactured by Oxford Magnet Technology LTD. (Witney, England) and customized gradient coil by Tesla Engineering Limited (Sussex, England). This magnet is independently ordered for the active shielded type with the weight of 11 tons. And, it is positioned within a magnetic shield constructed from annealed low carbon steel (grade 1006). Using a combination of superconductive shims located within the cryostat and resistive shims located in a specialized shim insert, the 3T magnet achieved a homogeneity of 3.78 ppm over a 40 cm diameter spherical volume established on 12-plane plot. The gradient system utilized in these studies consists of an asymmetric torque free gradient insert

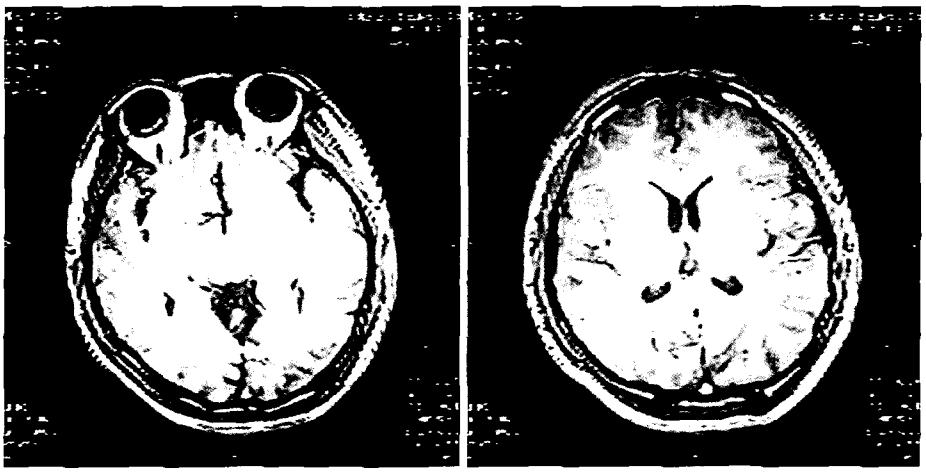

Fig. 1. Typical T1-weighted axial MR images in normal volunteer using conventional spin echo pulse sequence. Parameters are TR 500 ms, TE 10 ms, matrix 256 $\times$256, slice thickness 4 mm, FOV 20 cm, NEX 1.

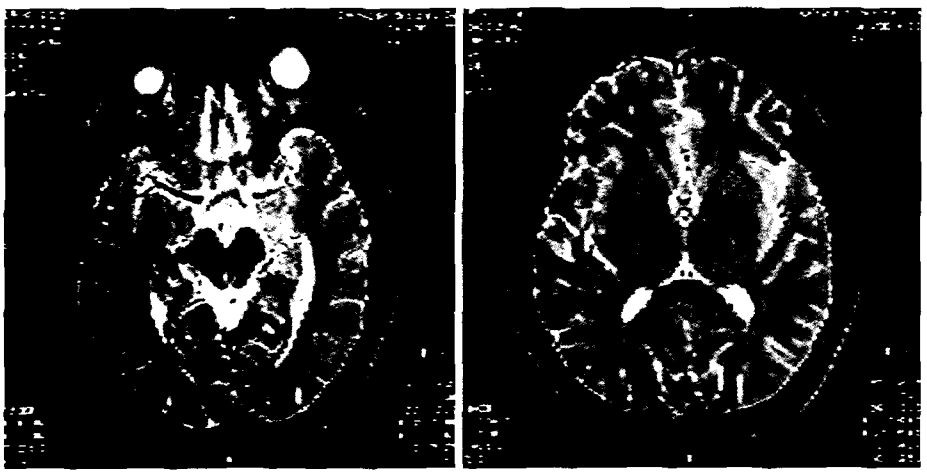

Fig. 2. Typical T2-weighted axial MR images in normal volunteer using fast spin echo with ETL 8. Parameters are TR 4000 ms, TE 108 ms, matrix 512$\times$512, slice thickness 5 mm, FOV 20 cm, NEX 2.

for whole body imaging. The gradient amplifier is capable of delivering 650V/430A on each gradient axis, and provided by MTS (MTS Systems Corporation, Horsham, PA, USA). And, spectrometer has a four channel system.

All images in this study were acquired with a Magnus 2.1 for Magnum 3T (Medinus LTD. Korea). It is equipped with Magnus Software and is able to support basic acquisition pulse sequences for fast EPI imaging, broad line imaging, 3D imaging, angiography and spectroscopy. The RF front end of the 3T system is comprised of a high power TR switch. Nonmagnetic narrow band Ga/As field effect transistor (FET) preamplifiers (Advanced Receiver Research, Burlington, CT, U.S.A) complete the front end allowing close proximity of the RF front end to the NMR coil. The quality of the receiver chain with the Magnum console was measured by examining the noise performance.

Spin echo (SE) pulse sequence was employed for T1-weighted MR images. However, for proton density and T2-weighted MR images, we used fast spin echo (FSE) with the echo train length of 8 or 16.

Radio frequency power at 128 MHz was provided by RF amplifiers constructed specifically for this project by AMT (Herley Company, Anaheim, CA, USA). Images were acquired with a birdcage volumetric head coil and TEM head coil. The TEM coil was designed to operate in quadrature and was constructed from a group of 16 TEM struts enclosed in a copper shield.

Results

T1-weighted axial SE images obtained from a brain of normal volunteer at 3T using TR 500ms, TE 10 ms and 256×256 matrix are displayed in Fig. 1. These images were obtained with a 4 mm slice thickness, a 20 cm FOV, using conventional SE pulse sequence. As can be

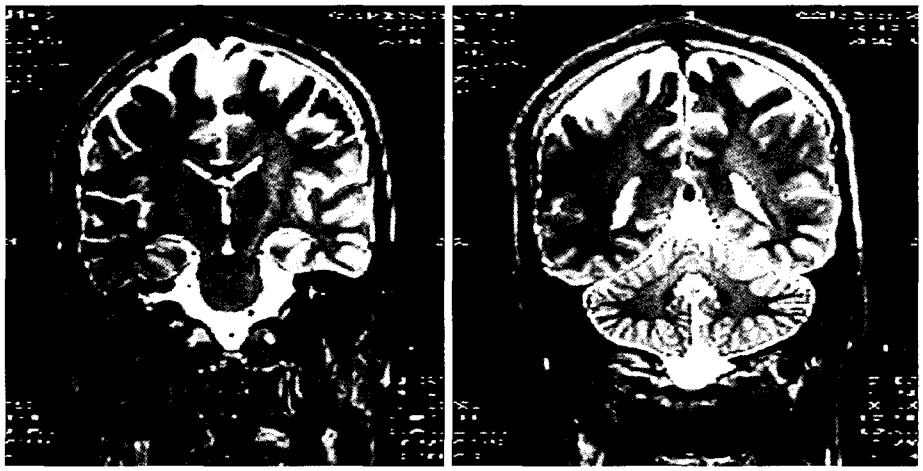

Fig. 3. T2-weighted coronal MR images in normal volunteer using fast spin echo with ETL 12.

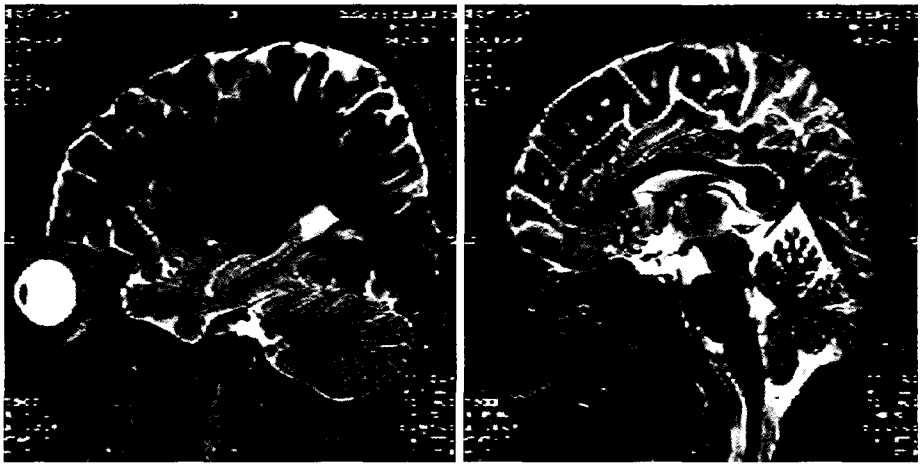

Fig. 4. T2-weighted sagittal MR images in normal volunteer using fast spin echo with ETL 8.

seen, the contrast between white and gray matter is remarkable. And, structures of basal ganglia, internal and external capsules as well as ventricles are well discriminated.

Figure 2 shows T2-weighted axial FSE images with high resolution of 512×512 matrix, TR 4000 ms, TE 108 ms. Note the substantial degree of vascular structure in detail. It is clearly differentiable for putamen and globus pallidus in basal ganglia. T2-weighted coronal and sagittal images are shown in Figs 3 and 4. Fine structural components in cerebellum are marked. Proton density axial images were shown in Fig. 5. For acquisition of proton density image, we used FSE by 4 excitation pulse with TR 2000 ms, TE 16 ms, NEX 2. White matter has rather dark signal than gray matter. Figure 6 shows fast spin echo FLAIR images with ETL 8, TI 140 ms, TR 6000 ms and TE 16 ms. CSF has completely dark signal than any other tissue. Most of fat signal was suppressed in fast spin echo STIR image in Fig. 7 with TI 2200 ms, TR 9000 ms and TE 96 ms. Note the fat tissue near skull has dark signal. MR angiography is presented by 3D-time of flight (TOF) technique with TR 30 ms, TE 6.6 ms, FA 25, NEX 1 in Fig. 8. Peripheral vessels as well as major vessels are clearly demonstrated without problematic artifacts.

T1 and T2-weighted coronal and sagittal MR images of knee are shown in Fig. 9 and 10, respectively. Lateral and medial meniscus are well denoted. For acquisition of T1-weighted coronal image, we used TR 500 ms, TE 17.4 ms, slice thickness 4 mm and NEX 1. And, T2-weighted sagittal images, we used FSE with ETL 16, TR 5500 ms, TE 88 ms, slice thickness 4 mm and NEX 1. Anterior cruciate ligament is well delineated as a dark signal intensity.

Figures 11 and 12 show T1- and T2-weighted MR image of foot with identical parameters for knee scans. The individual bones and joints are clearly seen.

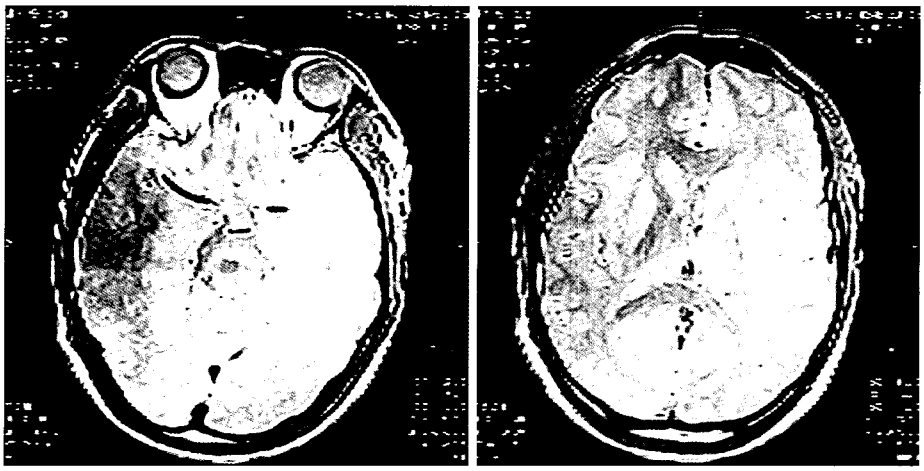

Fig. 5. Proton density axial MR images using fast spin echo by 4 excitation pulse with TR 2000 ms, TE 16 ms, NEX 2.

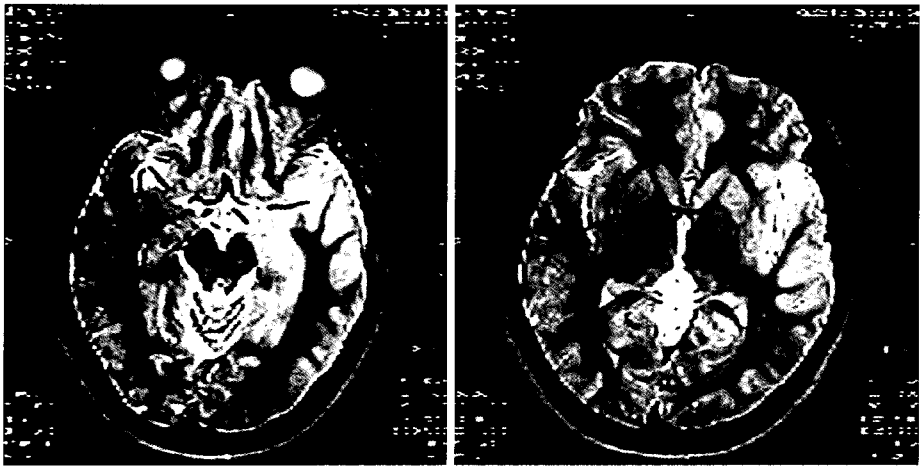

Fig. 6. Fast Spin Echo FLAIR images with TI 140, TR 6000 and TE 16, NEX 2.

T1, T2 and T2*-weighted MR images of wrist were obtained in Fig. 13. In particular, we used gradient echo of spoil pulse in steady state (GESPHSSF) with TR 450 ms, TE 15 ms, NEX 2 and flip angle 22°. The ligaments and muscle as well as entire carpal and metacarpal bones and joints are well visualized.

Discussion

Given the excellent technological performance of modern MRI scanners, the ability to acquire high resolution images with this modality is governed almost exclusively by available signal to noise. Thus, while excellent image scan be acquired at 1.5T, this field strength lacks the inherent signal to noise to make high resolution imaging feasible. As such, note that when conventional acquisition methods are utilized at 1.5T, it is difficult to obtain a resolution with a pixel volume much below 1 mm^3. Indeed, using a standard SE pulse sequence and a bird-cage quadrature head coil configuration with a state-of-the-art clinical scanner, images obtained with a 1 mm^3 pixel volume yielded little or no useful diagnostic information. In contrast at 3T MRI system, high resolution images (pixel volume $\leq$ 0.1 mm^3) can be obtained using standard imaging sequences and RF head coils without difficulty. This is the case despite the use of larger receiver bandwidths and less than fully relaxed spin excitation conditions.

T2-weighted MR image displayed in Fig. 2 was presented for appropriate reasons in that it represent the trial attempt to obtain high resolution results at 3T. In addition to provide high contrast of compatible quality in MR image, it dose reveal the potential of high field magnetic resonance imaging for increasing spatial resolution. While SNR of 3T system is increased approximately 2.7 times compared with prevalent 1.5T system, the contrast in 3T system was not proportionally increased like SNR. However, as SNR

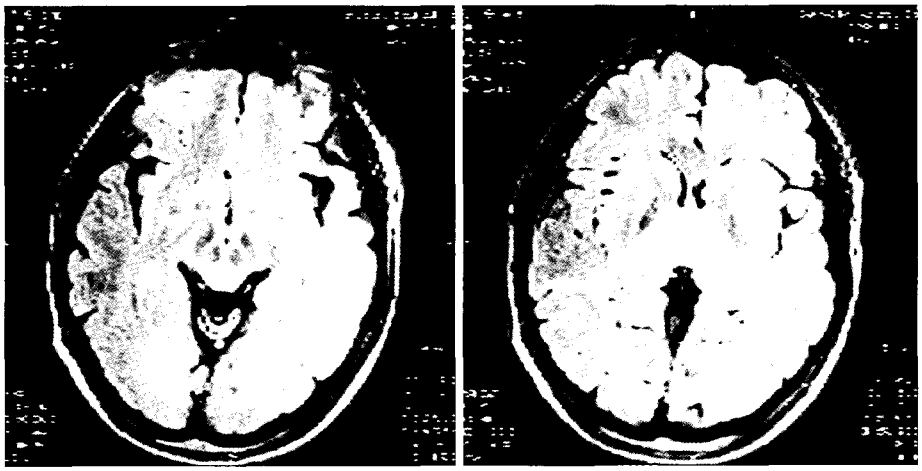

Fig. 7. STIR image for fat suppression with TI 2200 ms, TR 9000 ms, TE 96 ms, NEX 1.

Fig. 8. MR angiography is presented by 3D-time of flight (TOF) technique with TR 30 ms, TE 6.6 ms, FA 25°, NEX 1. Peripheral vessels are clearly demonstrated.

increase, the total scan time could be significantly reduced.

In addition to T1-weighted MR image (Fig. 1), T2-weighted MR images were displayed in Figs. 2-4. Note the vascular detail in these images, despite the use of a standard FSE pulse sequence. Much of this vascular anatomy is venous in origin. Nonetheless, there are literally hundreds of minute vessels visible in these images. This speaks to the tremendous potential of high field MRI system in obtaining high-resolution MRA

Fig. 9. T1-weighted coronal MR images of knee. Conventional spin echo pulse sequence was used. We used TR 500 ms, TE 17.4 ms, NEX 1, slice thickness 4 mm and rectangular FOV 160 × 180 cm.

Fig. 10. T2-weighted sagittal MR images of knee with FSE with ETL 16.

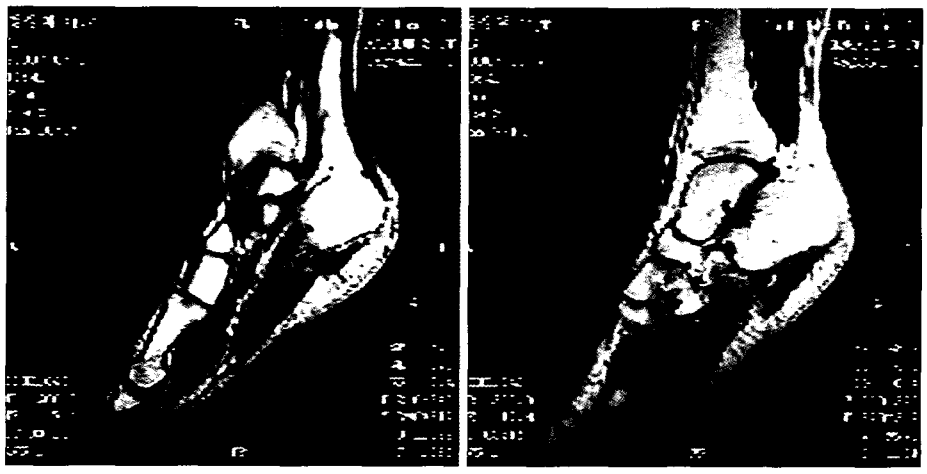

Fig. 11. T1-weighted sagittal MR images of foot. Parameters are identical with the scans for knee.

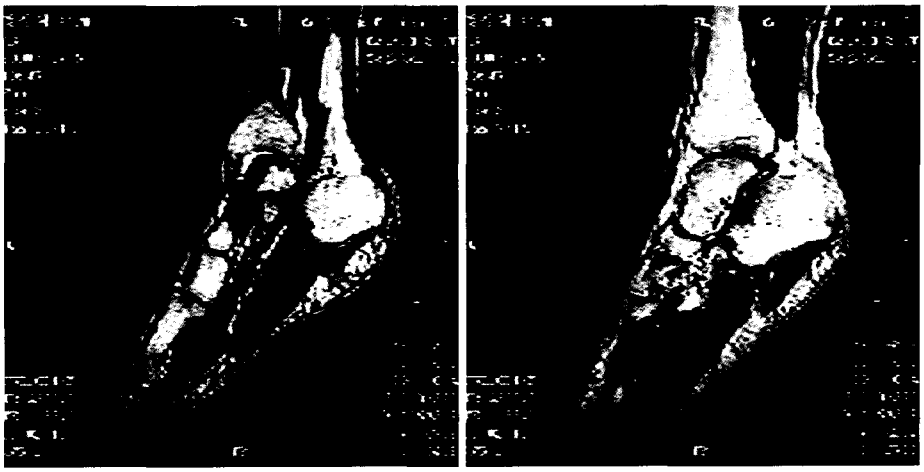

Fig. 12. T2-weighted MR image of foot.

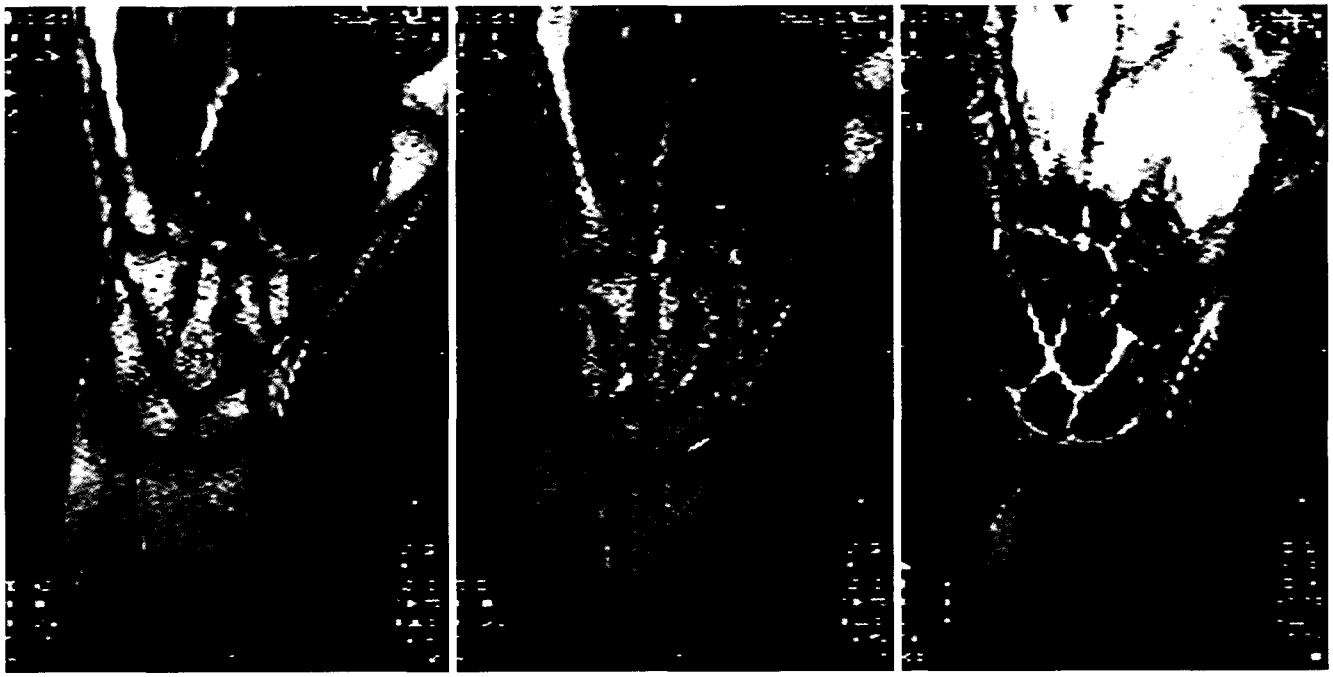

Fig. 13. T1, T2 and T2*-weighted MR images of wrist. In particular, we used gradient echo of spoil pulse in steady state (GESPHSSF) with TR 450 ms, TE 15 ms, NEX 2 and flip angle 22o. Total 10 segmental bone structures are well denoted.

results (Fig. 8). At the same time, while the pixel resolution on these images is outstanding, it cannot be directly related to true in-plane resolution due to inherent physiological motion. Thus, it may become important to gate image acquisition to cardiac or other physiological motion in order to help ensure that pixel resolution can be directly correlated to true resolution.

Nonetheless, the ability to obtain high resolution MR images will remain ultimately dictated by the Boltzmann equation. This equation determines the distribution of the spin population in the up state relative to the down state as a result of temperature and filed strength. Thus, given adequate spectrometer hardware, the only way to significantly enhance signal to noise is through a substantial increase in field strength.

The fundamental promise of high field MRI system relies on increased image resolution and decreased scanning times, both of which are critically related to intrinsic signal to noise (49). It reflects signal to noise in

the absence of T1, T2*, motion, flow, and scanner hardware effects. Intrinsic signal to noise, in turn must increase with field strength. It is clear from the images contained herein that the intrinsic signal to noise ratio at 3T will be phenomenal, possibly approaching a factor of 2.7 increase over a conventional 1.5T scanner. Given such performance, it is difficult to fully visualize the potential impact of high field MR image. Nonetheless, we had better insist the present trends in signal to noise and high resolution imaging continue. Finally it appears that the radiological sciences are destined to become increasingly field-strength oriented in nature.

Acknowledgment

We thank Hee-Keun Jee and all participants of CMC-Medinus 3T MRI project for their valuable assistance.

References

1. Damadian R, Goldsmith M, Minkoff L. NMR scanning. In: NMR basic Principles and Progress. vol. 19 Diehl P, Fluck E, Kosfeld R, eds. Berlin: Springer-Verlag, 1981:1-16
2. Lauterbur PC. Image formation by induced local interactions: example employing nuclear magnetic resonance. Nature 1973;242:190-191
3. Mansfield P, Chapman B. Active magnetic screening of gradient coils in NMR imaging. J Magn Reson 1986;66:573-576
4. Kumar A, Welti D, Ernst RR. NMR Fourier Zeugmatography. J Magn Reson 1975;18:69-83
5. Edelstein WA, Hutchison JMS. Spin warp NMR imaging and application to human whole-body imaging. Phys Biol Med 1990;25:751-756
6. Young IR, Cox IJ, Bryant D, Bydder GM. The benefits of increasing spatial resolution as a means of reducing susceptibility artifacts due to field inhomogeneities. Magn Reson Imag 1988;6:585-590
7. Abduljalil AM, Robitaill P-ML. Macroscopic susceptibility in ultra high field MRI. J Comput Assist Tomogr 1999;23:832-841
8. Venkatesan R, Haacke EM. Role of high resolution in magnetic resonance (MR) imaging: applications to MR angiography, intracranial T1-weighted imaging, and image interpolation. Int Imag Sys Technol 1997;8:529-543
9. Edelstein WA, Glover GH, Hardy CJ, Redington RW. The intrinsic signal-to-noise in NMR imaging. Magn Reson Med 1986;3:604-618
10. Parker DL, Gullberg GT. Signal to noise effciency in magnetic resonance imaging. Med Phys 1990;17:250-257
11. Hoult DI, Richards RE. The signal to noise of the nuclear magnetic resonance experiment. J Magn Reson 1976;24:71-85
12. Constable Henkelman RM. Contrast, resolution, and detectability in MR imaging. J Comput Assist Tomogr 1991; 15:297-303
13. Ackerman JJH, Grove TH, Wong GG, Grdian DG, Radda GK. Mapping of metabolites in whole animals by 31P NMR using surface coils. Nature 1980;283:167-170
14. Roemer PB, Edelstein WA, Hayes CE, Souza SP, Meuller OM. The NMR phased array. Magn Reson Med 1990;16:192-225
15. Mc Veigh ER, Henkelman RM, Bronskill MJ. Noise and filtration in magnetic resonance imaging. Med Phys 1985; 12:586-591
16. Ying K, Clymer BD, Schmalbrock P. Adaptive filtering for high resolution magnetic resonance images. J Magn Reson Imag 1996;6:367-377
17. Idy-Peretti I, Bittoun J, Alliot FA, Richard SB, Querleux BG, Cluzan RV. Lymphedematous skin and subcutis:in vivo high resolution magnetic resonance imaging evaluation. J Invest Dermatol 1998;110:782-787
18. Potter HG, Asnin-Ernberg L, Weiland AJ, Hotchkiss RN, Peterson MGE, McCormack RR. The utility of high-resolution magnetic resonance imaging in the evaluation of the triangular fibrocartilage compex of the wrist. J Bone Joint Surg 1997;79A:1675-1684
19. Drape JL, Peretti I, Goettmann S, Guerin-Surville H, Bittoun J. Standard and high resolution magnetic resonance imaging of glomus tumors of tose and fingertips. J Am Acad Dermatol 1996;35:550-555
20. Waldschmidt JG, Rilling RJ, Kajdacsy-Balla AA, Boynton MD, Erickson SJ. In vitro and in vivo MR imaging of hyaline cartilage: zonal anatomy, imaging pitfalls, and pathologic conditions. Radiograph 1997; 17:1387-1402.18-20
21. Majumdar S, Genant HK, Grampp SS, Newitt DC, Troung VHLin Jc, Mathur A. Correlation of trabecular bone structure with age, bone mineral density, and osteoporotic status: in vivo studies in the distal radius using high resolution magnetic resonance imaging. J Bone Mineral Res 1997; 12111-12118
22. Ouyang X, Selby K, Lang P, et al High resolution magnetic resonance imaging of the calcaneous: age-related changes in trabecular structure and comparison with dual X-ray absorptiometry measurements. Calcif Tissue Int 1997;60:139-147
23. Schmalbrock PM, Pruski J, Sun L, Rao A, Monroe J. Phased arry RF coils for high-resolution MRI of the inner ear brain stem. J Comput Assist Tomogr 1995;19:8-14
24. Brogan M, Chakeres DW, Schmalbrock P. High-resolution 3DFT MR imaging of the endolymphatic duct and soft tissue of the otic capsule. AJNR 1991;12:1-11
25. Arnold B, Jager L, Grevers G. Visualization of inner ear structures by three- dimensional high resolution magnetic resonance imaging. Am J Otol 1996;17:480-485
26. Dahm MC, Mack MG, Tykocinski M, Vogl TJ. Submillimeter imaging and reconstruction of the inner ear. Am J Otol 1997;18:S54-S56
27. Casselman JW, Kuhweide R, Deimling M, Ampe W, Dehaeme I, Meeus L. Constructive interference in steady

state-3D FT MR imaging of the inner ear and cerebellopontine angle. AJNR 1993;14:47-57
28. Ettl A, kramer J, DaxerA, Koornneef L. High-resolution magnetic resonance imaging of the normal extraocular musculature. Eye 1997;11:93-97
29. Mashima Y, Oshitari K, Imamura Y, Momoshima S, Shiga H, Oguchi Y. Orbital high resolution magnetic resonance imaging with fast spin echo in the acute stage of Leber's hereditary optic neuropathy. J Neurol Neurosurg Psychiatry 1998;64:124-127
30. Herrick RC, Hayman LA, Taber KH, Diaz-Marchan PJ, Kuo MD. Artifacts and pitfalls in MR imaging of the orbit: a clinical review. Radiograph 1997;17:707-724
31. Gass A, Barker GJ, MacManus D, et al. High resolution magnetic resonance imaging of the anterior visual pathway in patients with optic neuropathies using fast spin echo and phased array coils. J Neurol Neurosurg Psychiatry 1995;58: 526-529
32. Miloro M. Halkias LE, Slone HW, Chakeres DW. Assessment of the lingual nerve in the third molar using magnetic resonance imaging. J Oral Maxillofac Surg 1997;55:134-137
33. Dailiana T, Chakeres D, Schmalbrock P, Williams P, Aletras A. High resolution MR of the intraparotid Facial nerve and parotid duct. AJNR 1997;18:165-172
34. McGhee RB, Chakeres DW, Schmalbrock P, Brogan MA, Negulesco JA. The extracranial facial nerve: high resolution three-dimensional Fourier transform MR imaging. AJNR 1993;14:465-472
35. Laub GA, Kaiser WA. MR angiography with gradient motion refocusing. J Comput Assist Tomogr 1988;12:377-382
36. Paker DL, Paker DJ, Blatter DD, Du YP, Goodrich KC. The effect of image resolution on vessel signal in high resolution magnetic resonance angiography. J Magn Reson Imag 1996;6: 632-641
37. Laub GA, Kaiser WA. MR angiography with gradient motion refocusing. J Comput Assist Tomogr 1988;12:377-382
38. Barth M, Reichenbach JR, Vaenkatesan R, Moser E, Haacke EM. High-resolution, Multiple gradient-echo functional MRI at 1.5T. Magn Reson Imag 1999;17:321-329
39. Wald LL, Carvajal L, Moyer SE, Nelson SJ, Grant PE, Barkovich AJ, Vigneron DB. Phased array detectors and an automated intensity-correction algorithm for high-resolution MR imaging of the human brain. Magn Reson Med 1995;34:433-439
40. Feinberg DA, Kiefer B, Litt AW. High resolution GRASE MRI of the brain and spine: 512 and 1024 matrix imaging. J Comput Assist Tomogr 1995;19:1-7
41. Vaughan JT, Hetherington HP, Otu JO, Pan JW, Pohost GM. High frequency volume coils for clinical NMR imaging and spectroscopy. Magn Reson Med 1994;32:206-218
42. Pan JW, Vaughn JT, Kuzniecky RI, Pohost GM, Hetherington HP. High resolution neuroimaging at 4.1 T. Magn Reson Imag 1995;13:915-921
43. Vaughan JT, Hetherington HP, Otu JO, Pan JW, Pohost GM. High frequency volume coils for clinical NMR imaging and spectroscopy. Magn Reson Med 1994;32:206-218
44. Christoforidis GA, Bourekas EC, Baujan M, Abduljlil AM, Kangarlu A, Spigos DG, Chakeres DW, Robitaille P-ML. High resolution MRI of the deep brain vascular anatomy at 8 Tesla: susceptibility-based enhancement of the venous structures. J Comput Assist Tomogr 1999;23:857-866
45. Burgess RE, Yu Y, Christoforidis GA, Bourekas EC, Chakeres DW, Spigos D, Kangarlu A, Abduljalil AM, Robitaille P-ML. Human Leptomeningeal and cortical vascular anatomy of the cerebra cortex at 8 Tesla. J Comput Assist Tomogr 1999;23; 850-856
46. Robitaille P-ML, Abduljalil AM, Kangarlu A, et al. Human magnetic resonance imaging at 8 T. NMR Biomed 1998;11;1-3
47. Robitaille P-ML, Warner R, Jagadeesh J, et al. Design and assembly of an 8 Tesla whole-body MR scanner. J Comput Assist Tomogr 1999;23;808-820
48. Robitaille P-ML. Block-body and transverse electromagnetic resonators operating at 340 MHz: volume RF coils for ultra high field MRI. J Comput Assist Tomogr 1999;23:879-890
49. Edelstein WA, Glover GH, Hardy CJ, Redington RW. The intrinsic signal to noise in NMR imaging. Magn Reson Med 1986;3:604-618

대한자기공명의과학회지 5:138-148(2001)

3T 능동차폐형 전신 자기공명영상 장비로부터 얻어진 고해상도 자기공명영상

[1]가톨릭대학교 의과대학 의공학교실, [2]방사선과학교실, [3]메디너스 Co., [4]광운대, [5]고려대,
[6]한국과학기술원, [7]한양대, [8]동보시스템

최보영[1] · 강세권[1] · 추명자[1] · 백현만[1] · 김의녕[2] · 김범수[2] · 이재문[2] · 정성택[3] · 안창범[4]
오창현[5] · 김정호[6] · 김선일[7] · 이근남[8] · 이형구[1] · 서태석[1] · 이흥규[1] · 신경섭[1,2]

목적: 임상적용 가능시간 내에 세계 최초의 3T 능동차폐형 자석을 장착한 전신용 자기공명영상장비를 이용하여 고해상도의 자기공영영싱을 획득하였다.

대상 및 방법: 128 MHz의 공명주파수를 갖는 RF코일을 사용하여 정상인으로부터 스핀에코와 고속 스핀에코 펄스시퀀스를 적용한 두뇌, 무릎, 발 및 손목영상 등을 획득하였다. 전형적인 펄스시퀀스의 매개변수는 512×512 matrix, 20 cm FOV, 3 mm 절편두께, 1 NEX를 사용하였다. 특히 T1 강조영상을 위하여 TR=500 ms, TE=10 혹은 17.4 ms을 사용하였으며, T2 강도영상을 위하여 TR=4000 ms, TE=108 ms을 사용하였다.

결과: 3T의 신호대잡음비는 기존 병원에 설치된 1.5T에 비하여 2.7배 정도 향상되었다. 3T 자기공명영상은 매우 미세한 혈관 구조물을 표출하는데 도움을 주며, 또한 백질과 회질의 상당한 대조도를 제공하여 주었다.

결론: 본 연구결과에서 3T로부터 얻은 자기공명영상은 기존 1.5T 영상에서 얻은 영상에 비하여 더 높은 해상도와 민감도를 제공하여 주었다. 3T 고자장 자기공명영상에 나타난 증가된 신호대잡음비는 생체 조직단위의 영상을 획득하는데 유용하였다. 이러한 고해상도의 자기공명영상은 비침습적인 방법으로서 미세조직의 이상유무를 진단하는데 있어서 향후 더욱 임상에 도움을 주리라 예상한다.

통신저자 : 최보영, 가톨릭대학교 의과대학, 의공학교실, 137-040 서울시 서초구 반포동 505번지
Tel. 82-2-590-2427 Fax. 82-2-590-2425, E-mail: bychoe@cmc.cuk. ac.kr